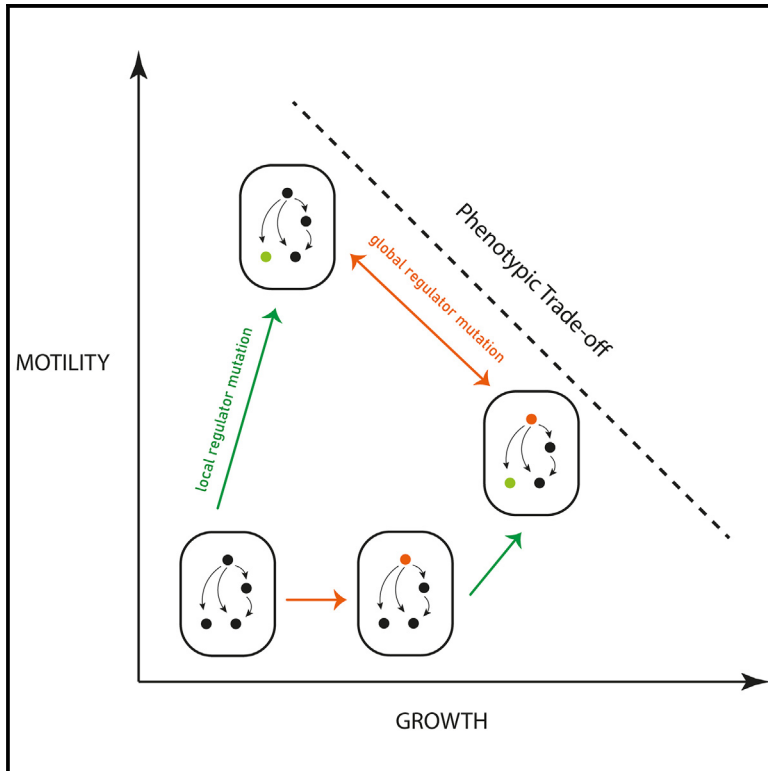# Global regulators enable bacterial adaptation to a phenotypic trade-off

Graphical abstract

Authors

Matthew Deyell, Vaitea Opuu,
Andrew D. Griffiths, Sander J. Tans,
Philippe Nghe

Correspondence

philippe.nghe@espci.fr

In brief

Microbiology; Evolutionary biology

Highlights

- Growth and motility both determine fitness but are in a trade-off

- Genetic perturbations in local regulators affect mostly motility

- Genetic perturbations in global regulators affect growth and motility simultaneously

- During evolution, global regulators are mutated last to tune the phenotypic trade-off

CellPress

iScience

Article

Global regulators enable bacterial adaptation to a phenotypic trade-off

Matthew Deyell,[1,2,3,4,8] Vaitea Opuu,[5,8] Andrew D. Griffiths,[1] Sander J. Tans,[6,7] and Philippe Nghe[1,5,8,9,*]

[1]Laboratoire de Biochimie, UMR CNRS-ESPCI 8231 Chimie Biologie Innovation, PSL Research University, ESPCI Paris, 10 Rue Vauquelin, 75005 Paris, France
[2]Department of Physiology, Biophysics, and Systems Biology, Weill Cornell Medicine, New York, NY, USA
[3]Meyer Cancer Center, Weill Cornell Medicine, New York, NY, USA
[4]Institute for Computational Biomedicine, Weill Cornell Medicine, New York, NY, USA
[5]Laboratoire de Biophysique et Evolution, UMR CNRS-ESPCI 8231 Chimie Biologie Innovation, PSL Research University, ESPCI Paris, 10 Rue Vauquelin, 75005 Paris, France
[6]AMOLF, Science Park 104, XG, Amsterdam 1098, the Netherlands
[7]Department of Bionanoscience, Kavli Institute of Nanoscience, Delft University of Technology, Delft, the Netherlands
[8]These authors contributed equally
[9]Lead contact
*Correspondence: philippe.nghe@espci.fr
https://doi.org/10.1016/j.isci.2024.111521

SUMMARY

Cellular fitness depends on multiple phenotypes that must be balanced during evolutionary adaptation. For instance, coordinating growth and motility is critical for microbial colonization and cancer invasiveness. In bacteria, these phenotypes are controlled by local regulators that target single operons, as well as by global regulators that impact hundreds of genes. However, how the different levels of regulation interact during evolution is unclear. Here, we measured in *Escherichia coli* how CRISPR-mediated knockdowns of global and local transcription factors impact growth and motility in three environments. We found that local regulators mostly modulate motility, whereas global regulators jointly modulate growth and motility. Simulated evolutionary trajectories indicate that local regulators are typically altered first to improve motility before global regulators adjust growth and motility following their trade-off. These findings highlight the role of pleiotropic regulators in the adaptation of multiple phenotypes.

INTRODUCTION

The fitness of cells depends on multiple phenotypes, but it is not always possible to optimize all of them simultaneously due to trade-offs.[1] A trade-off means that improving one trait may come at the cost of another. A key example is the trade-off between growth and motility, which has been demonstrated in bacteria and cancer cells.[2–6] For example, disseminated tumor cells are highly mobile, which promotes metastasis, but have a slow-cycling state that makes radiation therapy and chemotherapies poorly effective.[2] In bacteria, the trade-off between mobility and growth underlies the maintenance of population diversity through niche formation.[6,7] In the presence of a trade-off, evolutionary adaptation requires adjusting several phenotypes, either leading to specialization or a balance between traits.[8]

Here, we investigated the role of bacterial global regulators in coordinating multiple traits when these face a trade-off, and examined the evolutionary interplay between local and global regulators in the context of such a trade-off. Global regulators are defined as transcription factors that bind hundreds of operons, in contrast to local regulators that are dedicated to one or a few.[9] Global regulators are primarily characterized at the molecular level, based on the knowledge of their binding sites.[10] Due to the number and diversity of operons they regulate, global regulators are expected to alter several phenotypes. For instance, cAMP receptor protein (CRP) regulates the expression of secondary catabolites in response to cyclic AMP (cAMP)[11] and is implicated in biofilm formation.[12] Other global regulators (so-called nucleoid associated proteins or NAPs) such as the histone-like nucleoid structuring protein (HNS) and the factor for inversion stimulation (Fis) alter the compaction of the bacterial genome[13] depending on the growth phase,[14] and participate in the stress response[15] and biofilm formation.[16] However so far, studies of global regulators have focused on molecular mechanisms and a single phenotype.[17] Thus, how global regulators may coordinate multiple phenotypes in an evolutionary context is an open question.

To investigate the role of global regulators during adaptation to a phenotypic trade-off, we used a model system in which local and global regulators regulate growth and swimming in *E. coli*. CRISPR interference (CRISPRi) allowed us to knock down (denoted KD) transcription factors in combination, and hence study their genetic interactions. We chose 2 local (FlhDC and FliZ), 2 intermediate (mcaS and CsgD), and 3 global regulators
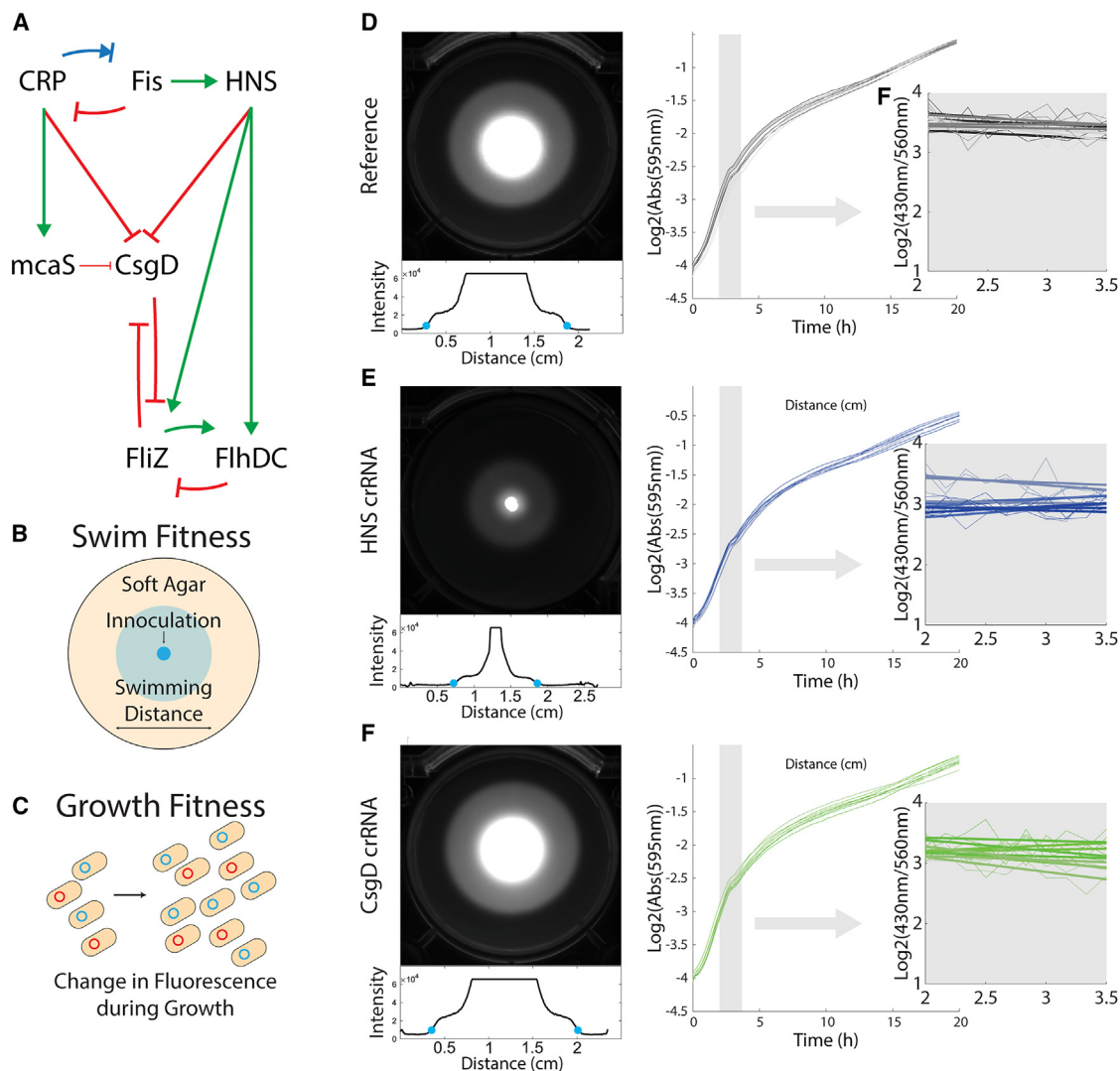
Figure 1. Quantification of swimming and growth

(A) Regulatory relationships between the selected panel of transcription factors. Each of these transcription factors was targeted with CRISPRi perturbation, either alone or in combination, and compared with a reference strain (RS) harboring a non-targeting crRNA.

(B) The swimming phenotype was determined through inoculation in the center of soft agar plates and measurement of the diameter up to the swimming front.

(C) The growth phenotype was determined as the change in fluorescence over time of the perturbation strain (cyan fluorescent) grown in competition with a reference strain (red fluorescent).

Phenotypic data for the RS (D) the HNS perturbation (E), and the CsgD perturbation (F). Left shows the direct image of the cells swimming in soft agar with the image analysis of the swimming photograph plotting the intensity of the bacterial signal, with the swimming front indicated by blue dots. The middle shows the growth curve in absorbance at 595 nm, with the exponential growth phase highlighted in light gray. The right shows the change in cyan vs. red fluorescence during the exponential growth phase. The slope is the relative growth phenotype.

(CRP, Fis, and HNS), known to regulate each other[10] (Figure 1A). The local regulators FliZ and FlhDC directly control the expression of the flagella operon essential for swimming mobility.[18] In contrast, the intermediate regulators indirectly control swimming mobility through acting on the local regulators. CsgD controls the expression of the Curli motility pathway and adhesion pili while repressing swimming.[19] CsgD is itself controlled by the small inhibitory RNA mcaS.[20] These mobility-regulating transcription factors are themselves regulated by upstream global transcription factors CRP, Fis, and HNS,[10] described above. This creates

a regulatory hierarchy between the transcription factors, with local regulators on the bottom directly controlling one phenotype, intermediate regulators above them, and finally at the apex are global regulators which control both lower levels and phenotypes directly.

Our approach allowed us to analyze the coupled variations of growth and swimming in response to KD of genes with different positions in the regulatory hierarchy (upstream, intermediate, or downstream), alone or in combination. We examined the genetic interactions (epistasis) between pairs of regulators and found

that epistasis differs between the two phenotypes and is modulated by the environment, demonstrating higher-order interactions. Despite this complexity, the phenotypic effects of genetic perturbations follow typical patterns when grouping genes by their position in the regulatory hierarchy: mutations in local regulators mostly improve swimming while global regulators adjust the balance between growth and swimming. Based on these measurements, we simulated evolution in variable environments where fitness depends on both phenotypes. We found that genetic changes in local and global regulators both contribute to improving fitness. However, genetic modifications are constrained by regulatory hierarchy: early evolutionary steps typically involve changes in local regulators, which are required to improve poor motility, whereas changes in global regulators tend to occur last, as only these allow fine-tuning the relative contribution of growth and motility.

RESULTS

Relation between genetic perturbations, phenotypes, and environments

We used CRISPRi to generate single and double knock down (KD) perturbations of 7 transcription factors (CRP, Fis, HNS, mcaS, CsgD, FliZ, and FlhDC). Cells were transformed with vectors expressing an inducible catalytically deactivated Cas9 (dCas9), mCerulean to fluorescently tag the cells, and a CRISPR RNA (crRNA) that targets the transcription start sequence of the relevant transcription factor (see Methods). CRISPRi represses gene expression by using the dCas9 as a programmable transcription factor.[21] We then quantified the swimming and growth phenotypes for this *E. coli* strain library (Figure 1), and the unperturbed reference strain (RS).

Swimming was quantified using a migration assay in 0.3% soft agar plates. Mobile bacteria form concentric bands while swimming in soft agar plates (Figures 1B, 1D–1F), driven by local nutrient gradients that form due to cellular consumption.[22,23] We quantified swimming as the diameter of the first swimming wave after 16 h in LB (Lysogeny Broth) media (rich) or 24 h in M63 lactose and M63 glucose media (minimal). Growth was quantified using a competition assay against a common unperturbed reference strain (RS).[24] This was done in microwell plates with constant shaking in these same media (Figures 1C, 1D–1F) using 3 signals: optical density, mCerulean fluorescence (emission 430 nm) of the query strain, and mCherry fluorescence (emission 560 nm) of the reference stain. The relative growth rate is computed as the slope of the logarithm of the ratio between fluorescence signals and is restricted to the exponential phase as controlled using optical density at 595 nm (OD for 'Optical Density'). This growth rate is normalized using the OD and fluorescent measurements to remove contributions due to differences between constructs and fluorescent markers, including maturation times, degradation rates, and expression costs (see Methods).

Swimming and growth were both measured over 9 replicates, consisting of 3 biological replicates (different days and initial colonies), each comprising 3 technical replicates (same day, different wells or plates). The swimming and growth values were taken as the median of all 9 measurements during the exponential growth phase and were highly reproducible (Figure 2A). Within each medium, differences between swimming and growth values across strains were significant, confirming the effectiveness of the KDs on these phenotypes (Figure 2A).

### Regulatory mutants are bound by a growth-motility trade-off

To understand how genetic perturbations impact phenotypes, we examined the distribution of phenotypes within the plane of the growth rate (x axis) and swimming distance (y axis) for all the strains, including single and double KDs (28 KD strains in total), in the 3 environments (Figure 2B). Single and double KDs cause mild to strong effects on both phenotypes, with growth rate changes ranging from $-0.17\ h^{-1}$ to $1.09\ h^{-1}$, and swimming diameter ranging from 0.4 cm to 3.4 cm after 16 h (see Table S1 for RS values). Growth is observed to increase or decrease due to genetic perturbations while swimming distance only decreases.

Environments have contrasting effects on the phenotypes. On the one hand, they alter the range of accessible growth values, which varies less for rich media (Figure 2B). Indeed, the largest changes in growth rates are observed in the poorest medium M63 Lactose (1.24-fold change), followed by M63 Glucose (0.97) and finally LB (0.32). On the other hand, the range of accessible swimming performances is quite similar across environments. The best-performing strain in LB swims 0.35-fold and 0.25-fold further than the best strains in M63 with glucose and lactose media, respectively.

Moreover, the distribution of genetic variants in the phenotypic space of Figure 2B displays a trade-off: some mutants have a growth rate higher than the unperturbed RS (squares in Figure 2B) but at the expense of deteriorated swimming. This trade-off between growth and swimming was formerly characterized in experimental adaptive evolution experiments and mutants.[25,26] Such trade-offs can be analyzed using the concept of Pareto optimality,[8] where organisms that cannot be outcompeted on all functions simultaneously are said to be Pareto optimal. In Figure 2B, Pareto optimal strains are those where no other strain grows more without swimming less. Pareto optimal strains localize on a line called the Pareto front [1]. Respectively 4, 6, and 3 Pareto-optimal strains are observed in LB, M63 Glucose, and M63 Lactose (solid symbols in Figure 2B).

The coupling between phenotypes depends on gene hierarchy

To analyze the relationship between regulatory network structure and phenotypic effects, we first examined whether changes in growth and swimming were associated with the specific genes being perturbed (Figure 3). Each panel of Figure 3 reports the phenotypic effects of a given KD across all genetic backgrounds and environments. A vector along the x axis means the KD affects growth only, while a vector along the y axis means the KD affects swimming only. Diagonal vectors indicate pleiotropy, in other words, a coupling between growth and swimming. If the coupling is positive, growth and swimming both improve (top-right quadrant) or both deteriorate (bottom-left quadrant). If the coupling is negative, improved growth comes at the expense of deteriorated swimming (bottom-right quadrant), or vice
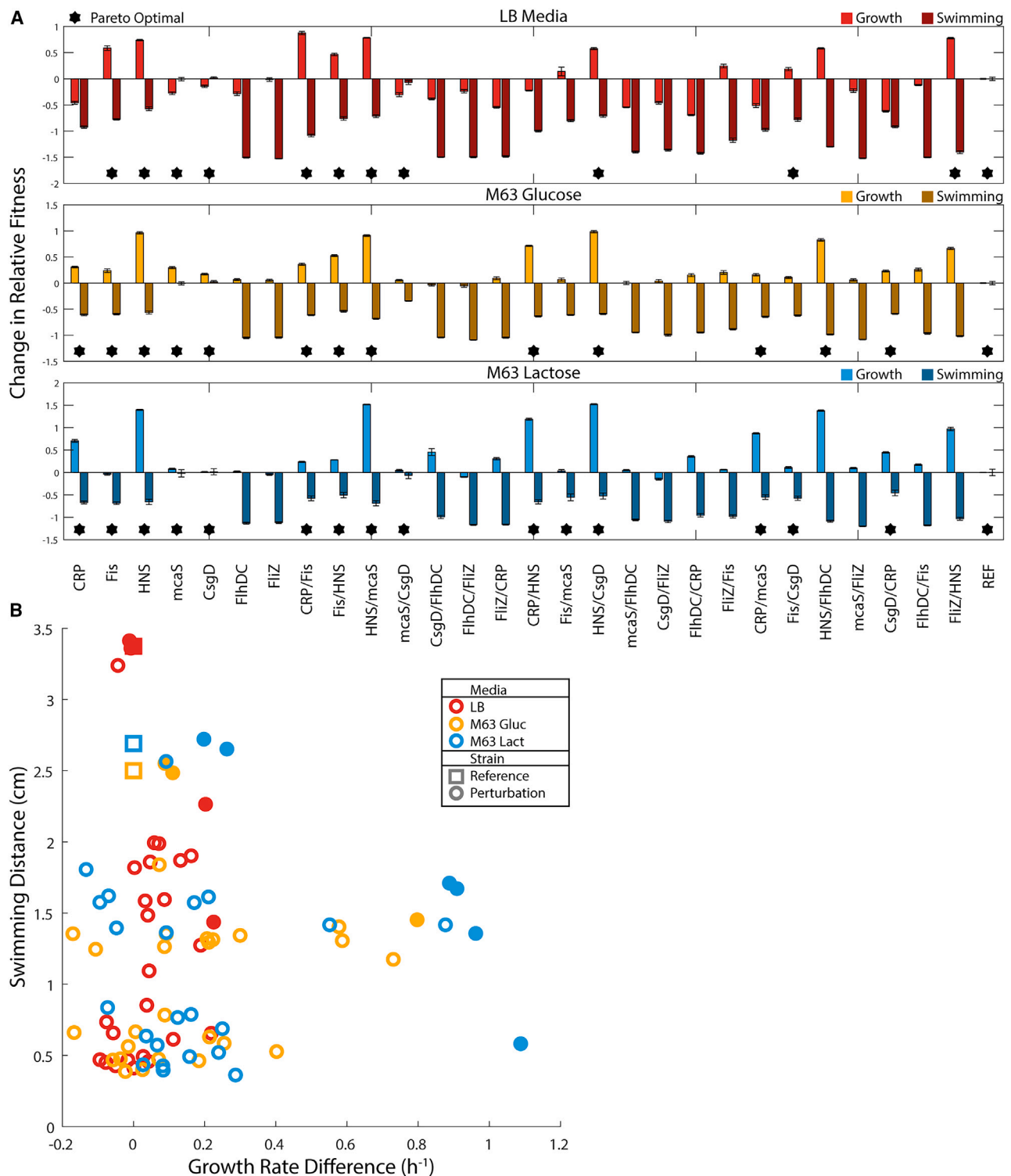
Figure 2. Growth-swimming phenotype space displays a Pareto front

(A) Median values for growth and swimming fitness, normalized to the reference strain (*n* = 9). Growth for each CRISPRi perturbation grown was in competition with non-targeting reference for 20 h. Swimming distance was measured in soft agar after 16 h. Error bars represent SEM (standard error of the mean). Pareto optimal strains within each media are marked with a star and are defined as any strain in which no other strain has significantly higher ($p < 0.05$) growth and swimming fitness. (B) The distance that each strain can swim (in 16 h for LB or 24 h for M63) is plotted against the growth rate difference with the RS (squares) for each KD strain (circles). Solid symbols are Pareto optimal strains.
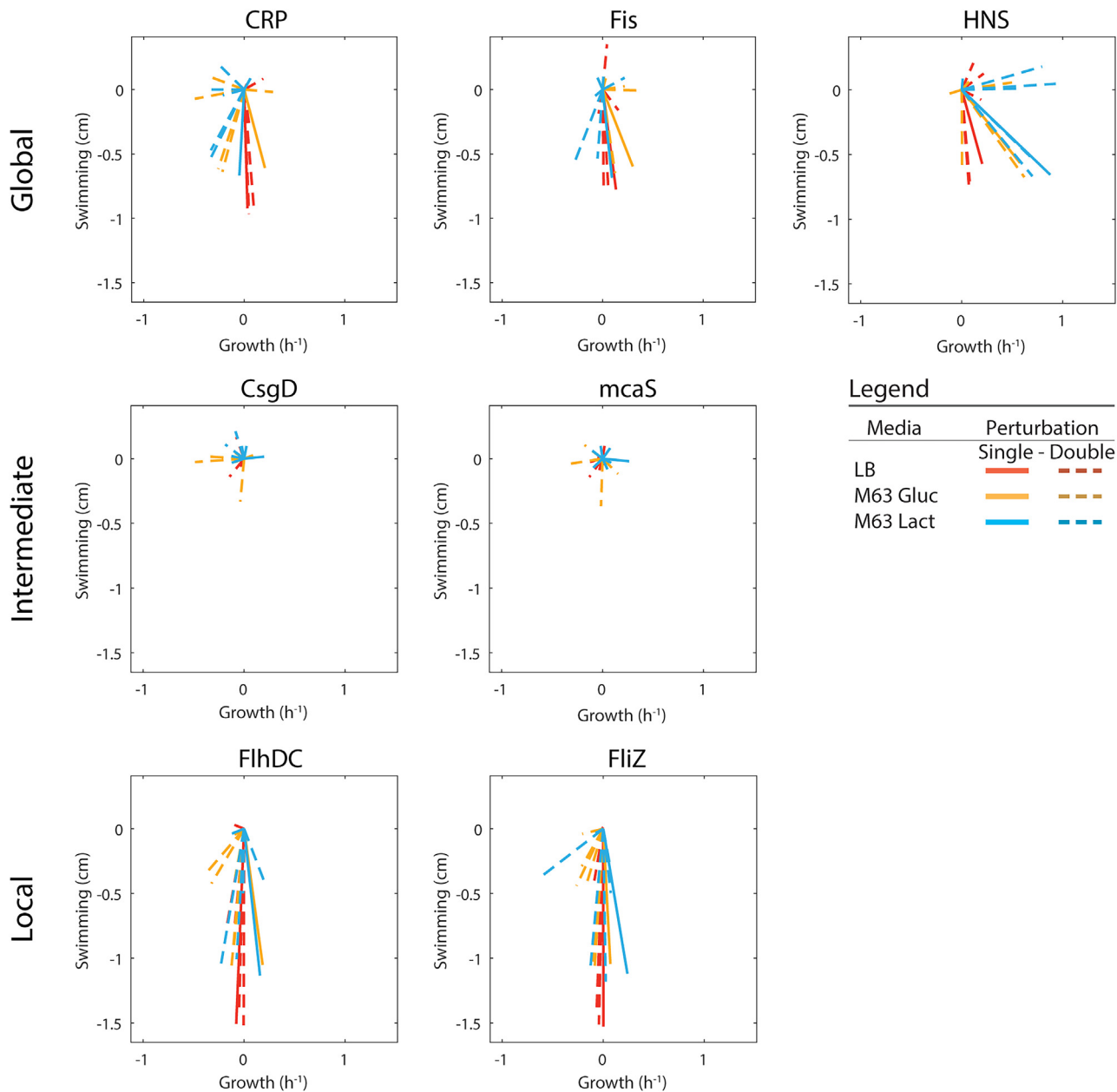
Figure 3. Impact of regulatory structure on the magnitude and direction of phenotypic effects
The vectors represent the phenotypic difference in the growth-swimming space for each given KD, where the strain without the KD is at the origin irrespective of its genotype. If the KD is the only perturbed gene in a genotype, it is represented as a solid line (Single). If there is another perturbation in the same genotype, it is represented as a dashed line (Double). The top row contains all the global regulators, the middle row contains the intermediate regulators, and the bottom row contains the local regulators.

versa, growth deteriorates while swimming improves (top-left quadrant).

KDs yield a varying range of couplings between phenotypes depending on the gene being perturbed. CRP, Fis, and HNS show the most diverse responses to their KD, where different genetic backgrounds and environments lead to changes in growth exclusively, swimming exclusively, or both (Figure 3). Perturbations of mcaS and csgD also had varied effects but were of

low magnitude as the majority are not statistically significant ($p > 0.05$, Welch's t-test, $n = 9$). In contrast, FliZ and FlhDC had strong effects on motility regardless of the environment but showed a mild positive or negative impact on growth.

The three classes of responses described above correspond to different positions of the regulators within the regulatory network hierarchy (Figure 1). CRP, Fis, and HNS are upstream global regulators. Together, they accounted for 69% of
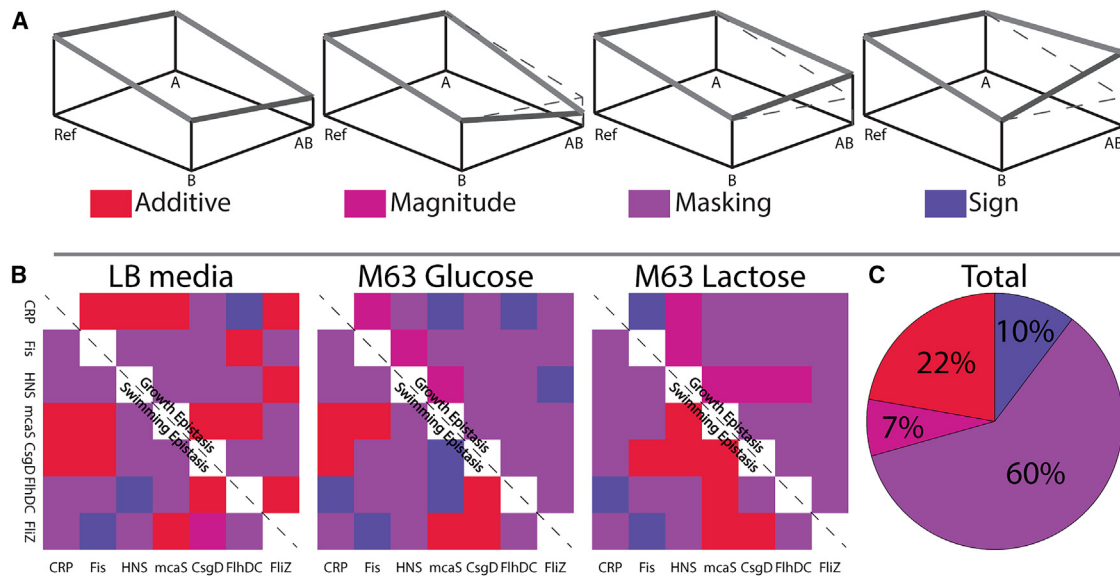
Figure 4. Epistasis between regulatory gene knock-downs

(A) Additive case (no epistasis, parallel edges): mutation A has the same effect irrespective of the background (RS or mutant B), and mutation B has the same effect irrespective of the background (wild-type [ref] or mutant A). Magnitude epistasis: the effect of mutation A is increased or decreased by the presence of mutation B, but the direction of the effect is the same (same for mutation B in the presence or not of mutation A). Masking epistasis: mutation A has no effect in the presence of mutation B. Sign epistasis: the direction of the effect of mutation A is changed by the presence of mutation B.

(B) Calculated Epistasis for each fitness metric in each growth media, with Growth epistasis above the diagonal and Swimming epistasis below. Epistasis was calculated as described in Figure 4. The total number of conditions tested is 126, $n = 9$.

(C) Epistasis statistics observed across all perturbation pairs and media.

perturbations that show negative growth-motility coupling (vectors that point top-left or bottom-right in Figure 3), mostly caused by HNS ($n = 16$). Such negative couplings are of particular interest as they are manifestations of the growth-motility trade-off. The regulators with the mildest effects, mcaS, and csgD, occur in an intermediate position in the network hierarchy. Finally, FliZ and FlhDC had the strongest impact on swimming but little impact on growth. This is consistent with their position as downstream transcription factors dedicated to flagella regulation. FliZ and FlhDC accounted for 60% (6/10) of the few cases where swimming and growth both phenotypes decreased (7% of all perturbations).

This analysis indicates that the downstream local transcription factors mostly modulate swimming, as may be expected. However, the upstream global transcription factors couple growth and swimming in a variety of ways. For example, swimming and growth may both increase or decrease together, move in opposite directions, or vary independently. However, it remains unclear at this stage how the diversity of effects caused by perturbations in global regulators leads to the distribution of phenotypes observed in Figure 2B.

Genetic interactions are high-order but consistent with regulatory hierarchy

To understand the influence of regulatory interactions on phenotypic effects, we first examined the epistasis between each pair of transcription factors,[27] which quantifies the departure from additive effects. Epistasis may take various forms including magnitude or sign epistasis (Figure 4A). Magnitude epistasis

conserves the sign of the fitness effect across backgrounds but not the amplitude of the effects. We denote here the extreme form of magnitude epistasis as 'masking epistasis', in which a genetic perturbation has no further effect if another perturbation has already occurred (by the classical definition of phenotypic epistasis). Sign epistasis refers to the case where a mutation causes a fitness increase in one background but a decrease in another background. When sign epistasis applies to both genes being perturbed, it is referred to as reciprocal sign epistasis.

In total, we categorized 126 epistasis interactions, resulting from 21 gene pairs for two phenotypes across three environments (Figures 4B and 4C, detailed in Figures S1–S3). Epistasis is pervasive with only 22% of gene pairs showing additive effects across all environments for both phenotypes (Figures 4B and 4C). Epistasis generally differs for growth and mobility phenotypes: over 21 gene pairs, epistasis differs between growth and motility in 17 cases in LB, 13 cases in M63 Glucose, and 13 in M63 Lactose (compare the color of the squares positioned symmetrically across the diagonal in Figure 4B). This observation is consistent with the two phenotypes being differentially regulated by the same regulatory network and shows that the wiring between genes is not the only determinant of epistasis.[28,29] Furthermore, genes display a higher-order effect with the environment: for a given gene pair and a given phenotype, epistasis differs in at least one of the 3 environments in 27 over 42 cases, consistent with other studies.[30]

The above analysis reveals complex genetic interactions but not any obvious relationship between genes, phenotypes, and environments. However, examining the combined effects of
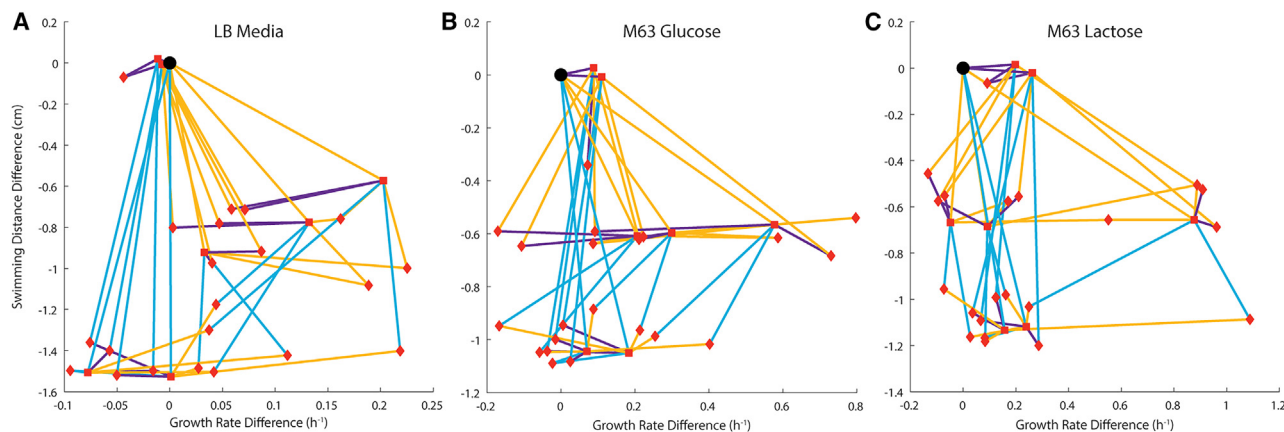
Figure 5. Relationship between regulatory network structure and response in phenotype space

The trajectories for each perturbation are colored by the group of the transcriptional regulator: Global (yellow), Intermediate (Purple), or Local (blue). The reference strain is represented as a black circle, single perturbations are represented as a square, and double perturbations are represented as a diamond. In all three environments, genotypic modifications in local motility regulators connect poor swimmers (low yvalues) to better swimmers (vertical or nearly vertical blue lines). Genotypic modifications in intermediate regulators typically lead to changes in growth (horizontal purple lines). Genotypic modifications in global regulators either affect growth for poor swimmers (yellow horizontal lines at low yvalues), or jointly modulate growth and swimming (yellow oblique lines for upper yvalues).

gene KDs in the joint space of growth and swimming (Figures S1–S3) points to typical patterns when grouping genes as upstream (global regulators CRP, Fis, HNS), intermediates (mcaS, CsgD), and downstream (local regulators FlhDC, FliZ). For instance, interactions between upstream and other upstream or intermediate genes (first 3 columns, top 5 rows in Figures S1–S3) lead to triangular patterns. Interactions between upstream and downstream genes (first 3 columns, bottom 2 rows) tend to yield larger perturbations in both swimming and growth as compared to interactions between other ensembles. Interactions between downstream genes (bottom 2 rows) and other downstream intermediate genes (last 4 columns) are dominated by a strong decrease in swimming with little impact on growth.

The insight gained from the hierarchical grouping of genes invites us to re-examine the overall set of perturbations in the phenotypic space (Figure 5). We colored each edge by which of the three gene groups was affected by the genetic perturbation: upstream global (yellow), intermediate (purple), or downstream local (blue) regulators. In this representation, the overall structure of gene perturbation effects appears consistent across environments (Figures 5A–5C) even though epistasis for a specific pair of KDs may not be (Figures 4 and S1–S3). In Figure 5, we observe that significant changes in swimming (vertical edges) are mainly attributed to local (blue) or global (yellow) perturbations. Significant changes in growth (horizontal edges) mostly occur via global regulators (yellow) irrespective of the swimming value, and intermediate regulators (purple) for strains that swim moderately well. Positively coupled changes in phenotypes (oblique edges with a positive slope) occur mostly via local regulators, starting from low swimming strains. Negatively coupled changes in phenotypes (oblique edges with a negative slope) occur almost only via global regulators, and trade swimming for growth.

Overall, local regulator perturbations mostly connect strains which perform poorly at both phenotypes to strains near the Par-

eto front, which are either good swimmers or moderate swimmers with large growth. In contrast, global regulator perturbations have a strong effect on growth in the low swimming region, but trade swimming for growth in the Pareto front region. The trajectories of Figure 5 show that, when starting from a genotype with poor motility and growth, evolution of both local and global regulators can improve one phenotype or the other. However, such an evolutionary optimization faces constraints: improving motility requires changes in local regulation at some point (blue lines in Figure 5), but adjusting the relative performance of motility and growth along the Pareto front can only be done by changes in global regulators (yellow lines in Figure 5).

Evolution under complex selection pressures involves local and then global regulators

To investigate the role of local and global regulators during adaptation, we computed evolutionary trajectories in variable environments where fitness depends on the two phenotypes. We consider here the regime where environments vary on timescales longer than the typical time for mutations to fixate. For simplicity, we call 'mutation' any genotypic perturbation which may correspond to a loss of function (KD) or a gain of function (KD taken in reverse, or knock-up KU). Mutations perturb the two phenotypic values, growth and motility, which are experimentally found to display trade-offs for all pairs of mutations (Figure 2B).

To simulate the evolution over the four mutations and associated phenotypic values, we consider all possible scenarios where growth and swimming may have more or less relative importance for fitness. For this, we vary a parameter λ that linearly weights the contribution of growth and swimming: When $\lambda = 0$, only swimming determines fitness; When $\lambda = 1$, only growth determines fitness; For intermediate values of λ, both growth and swimming contribute to fitness, but growth contributes more for larger λ. When $\lambda = 0$, we defined the positive contribution of swimming to fitness using a sigmoidal function of the swimming
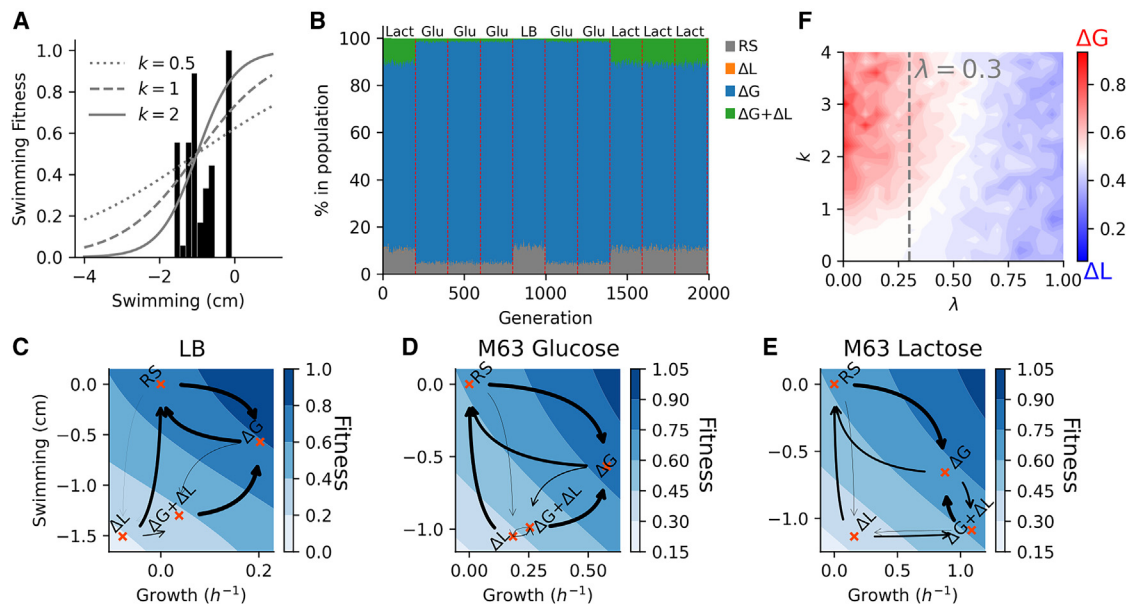
Figure 6. Evolution in variable environments

(A) Distribution of swimming distance (histogram) and examples of swimming-to-fitness relationships, computed as a sigmoid of the swimming distance parameterized by a steepness parameter k, here centered on s0 = −1 cm.

(B) Example of evolutionary trajectory between the 4 genotypes (RS, ΔL, ΔG, ΔL+ΔG) generated by HNS and FlhDC knock-outs in a variable environment randomly alternating between LB ('LB'), M63 Glucose ('glu') and M63 Lactose ('lact') every 200 generations.

(C–E) Mutational trajectories for the HNS-FlhDC in the three environments. Arrow thickness is proportional to the rate of transition during evolution. The fitness landscape is depicted by a gradient of blue.

(F) Proportion of local and global mutations as a function of k and λ (s0 = −1 cm), where the color scale indicates the proportion of ΔG mutations (from blue, with only ΔL mutations, to red, with only ΔG mutations).

distance with parameters s_0 and k (Figure 6A). The parameter s_0 is the typical swimming distance difference with the reference strain allowing survival, which we set to −1 cm, the middle of the range of the measured values (a higher or lower s_0 would make swimming differences irrelevant to selection). The parameter k determines the sigmoid sharpness, where a very small k makes the response flat (no impact of swimming) and a very large k tends to a step function (threshold selection). When λ = 1, fitness is taken as the differential growth rate normalized over the range of growth in a given medium. Intermediate values of λ interpolate between swimming and growth fitness functions. We explored the regime of strong selection for evolutionary trajectories within the 6 landscapes generated by KD pairs comprising a global regulator (CRP, Fis, or HNS) and a local regulator (FlhDC or FliZ). For each landscape, we used the experimentally measured phenotypic values of the 4 genotypes and simulated evolutionary trajectories in an environment that varies randomly between the three media, as exemplified for the pair HNS-FlhDC in Figure 6B. The starting genotype is taken randomly for each realization of the simulation, which allows us to record statistics of the mutational paths over all possible adaptation scenarios. Populations rapidly reach an equilibrium between mutation and selection after each environmental change, where they display small fluctuations around average proportions between genotypes (Figure 6B).

We first focused on regimes where the contributions of growth and swimming to fitness are well-balanced. This is realized

around λ = 0.3, where the fitness range is similar on the x and y axes (equivalently, isofitness lines are oblique, see Figures 6C–6E for the pair FlhDC-HNS; Figure S4B for all pairs). In the following, ΔL denotes the strain with a local regulator KD, ΔG the strain with a global regulator KD, and ΔL+ΔG the double KD. Figures 6C–6E and Figure S4 depict the mutational landscapes in different environments and for different choices of local-global regulator pairs, with arrows representing mutations between genotypes. The thickness of the arrows is proportional to the probability of mutating from one genotype to another.

We observe typical trajectories that are reproduced between all mutational landscapes. For instance, in panels, C-E of Figure 6, thick arrows depart from the ΔL and ΔL+ΔG genotypes, but those genotypes have weak incoming arrows. This indicates that ΔL and ΔL+ΔG are populated only transiently and tend to evolve irreversibly toward other genotypes. In contrast, the RS and ΔG genotypes have strong incoming and outgoing arrows, indicating that evolution can occur back and forth between those two genotypes located on the Pareto front (Figures 6C–6E). The dynamics just described in the case of the HNS-FlhDC pair are also observed in 14 of the 18 landscapes (Figure S4B), with first a knock-up of the local regulator (from ΔL to RS or from ΔL+ΔG to ΔG, depending on the starting genotype), then an exchange between the RS and the ΔG genotypes via the global regulator. Exceptions occur in lactose, with the above-mentioned FlhDC-HNS pair which includes the ΔL+ΔG genotype on the Pareto front (Figure 6E) and the pairs FlhDC-CRP, FliZ-CRP, and

FliZ-Fis, which display collapsed trajectories dominated by an exchange between ΔL and RS (Figure S4B). Nevertheless, genotype exchange via the global regulator is the dominant mode of long-term evolution in variable environments, as confirmed on average over all simulated evolutionary trajectories (Figure 5F, λ = 0.3), as well as for each pair considered separately (Figure S4, λ = 0.3).

In regimes where fitness is dominated by growth or swimming, the local or global regulator may be the ultimate target of adaptation. Fitness is dominated by growth when k is close to 0 or λ is close to 1 (Figure S4A). In these cases, mutations in local regulators dominate (Figures 6F and S5), due to genotypes with maximal growth being in large majority ΔG, with ΔL+ΔG coming second, both exchanging via a local regulator mutation (12 over 18 pairs over the 3 media, Table S2 and Figure S5). In contrast, fitness is dominated by swimming when k is not too small and λ is close to 0 (Figure S4C). Mutations occur mostly in the global regulator (Figures 6F and Figure S5) due to the RS swimming the furthest and the ΔG coming second (Figure S4C).

DISCUSSION

Transcription factors CRP, HNS, and Fis are global regulators that regulate hundreds of operons in bacteria.[10] They have been detected by large-scale mapping of binding sites and are known to be implicated in various phenotypes, such as metabolism, biofilm formation, and motility.[31] Furthermore, global transcription factors are frequently modified when bacteria undergo directed evolution in unforeseen complex environments.[32] Overall, this hints at their role in adapting to multiple phenotypes. However, few studies have examined the impact of evolutionary perturbations when multiple phenotypes determine fitness. On the one hand, evolutionary constraints in gene networks are generally studied for single traits. On the other hand, studies that examine multiple traits focus on the best-adapted strains that are Pareto optimal. Therefore, the contribution of global regulators during adaptation to a phenotypic trade-off remains poorly understood.

Here, using genetic perturbations in *E. coli*, we have shown that global regulators help adjust the relative contribution of growth and swimming, when those two phenotypes reach nearly optimal values. This is important because there is a trade-off between growth and swimming which requires a mechanism to tune the balance between these two phenotypes depending on selective pressures. Additionally, our analysis of evolutionary scenarios shows that global regulators may not act alone: they must interplay with local regulators that are required in early evolutionary steps to improve the swimming phenotype.[33] The model we studied is likely typical for regulatory architectures, at least in the case of *E. coli*, whose regulatory network was shown to be mainly composed of hierarchical regulatory motifs with 2 or 3 layers, where global regulators regulate intermediate then local regulators, the latter being specific to single operons.[9]

These findings invite us to reconsider possible explanations for the origin of global regulators. One explanation is that they are regulatory 'hubs' that result from a random process of network wiring.[34] Network hubs can result from the rule of preferential attachment, where transcription factors targeting many genes have more chance to regulate newly appeared genes than those dedicated to a single operon (e.g., following gene duplication-divergence events).[35] However, it is unclear whether such a network wiring process makes sense in the context of selection.

A contrasting explanation of global regulators is that the co-regulation of operons by global and local regulators reflects cellular decision-making. For instance, alternative sugar operons are triggered only in the absence of glucose when CRP is activated. This is the case of the lac operon, which additionally requires the allosteric suppression of LacI repression in the presence of lactose. The underlying rationale is a prioritization between carbon sources depending on their quality to ensure optimal metabolic efficiency.[36] Even though HNS and Fis may potentially follow a similar logic, for example, triggering biofilm formation as a function of the growth phase, this has not been demonstrated. Global regulation may also come with an evolutionary cost due to their highly pleiotropic character, as mutating them can cause a large number of deleterious effects.[37]

The present study highlights an additional ingredient central to complex adaptations: the existence of phenotypic trade-offs. Such phenotypic trade-offs are common and have been observed in complex diseases,[38,39] including aggressive brain cancers[40] and metastatic solid tumors.[2] These traits have been linked to highly pleiotropic regulators such as c-myc and NF-kB.[41–43] While specific mutations have been shown to optimize cancer toward a specific trait,[44] there lacks any clear mutational drivers for metastasis in general.[45] Understanding how phenotypes, such as mobility and growth, are coupled and evolve has become a critical question in health sciences. Adaptation in the presence of trade-offs is complex because of the requirement of simultaneous and coordinated optimization of multiple phenotypes. Evolution becomes dependent on genetic changes that couple variations in multiple phenotypes.[46] In this context, accessible evolutionary trajectories require some degree of pleiotropy, as we observed when only global regulators can adjust two optimal phenotypes. Pleiotropy may be a necessary evil to adapt to phenotypic trade-offs, thus illustrating how network complexity may find its roots in functional complexity.[47]

Limitations of the study

Genetic perturbations considered here consist of knock-down. Whether the findings are preserved for mutations with intermediate effects, or for complete knock-out with stronger effects needs to be tested. Other evolutionary may be studied, such as weak selection, in which case the order of mutations is expected to be less constrained. An exciting perspective is to leverage the CRISPRi approach in high-throughput bar-coded screens and examine the generality of the local–global impact of regulators at a genomic scale.

Materials availability

Plasmids generated in this study have been deposited to Addgene, Deposit 85178.

Data and code availability

- Codes of simulations and figure production are available for download at Zenodo at https://doi.org/10.5281/zenodo.10201172.
- Data for figures can be downloaded at Zenodo https://doi.org/10.5281/zenodo.10201172, and the underlying raw data are available upon request to the lead contact.
- Other resources (including oligonucleotides, strains and chemicals) are available from commercial providers as indicated in the key resources table.

AUTHOR CONTRIBUTIONS

Conceptualization: M.D., V.O., S.T., and P.N.; Methodology: M.D., V.O., A.G., and P.N.; Formal analysis: M.D, V.O., and P.N.; Investigation: M.D. and V.O.; Writing–original draft: M.D., V.O., and P.N.; Writing–editing: M.D., S.T., A.G., and P.N.; Visualization: M.D. and V.O.; Supervision, administration, funding: P,N.

DECLARATION OF INTERESTS

The authors declare no competing interests.

STAR★METHODS

Detailed methods are provided in the online version of this paper and include the following:

- KEY RESOURCES TABLE
- EXPERIMENTAL MODEL AND STUDY PARTICIPANT DETAILS
  - Microbe strains used
  - Growth conditions of cultures
- METHOD DETAILS
  - Creation of vectors
  - Growth competition assays
  - Swimming assays
- EVOLUTIONARY SIMULATION
  - Code
- QUANTIFICATION AND STATISTICAL ANALYSIS
  - Computation of relative growth rates
  - Statistical methods used

SUPPLEMENTAL INFORMATION

Supplemental information can be found online at https://doi.org/10.1016/j.isci.2024.111521.

REFERENCES

1. Roff, D.A., and Fairbairn, D.J. (2007). The evolution of trade-offs: where are we? J. Evol. Biol. 20, 433–447.

2. Gallaher, J.A., Brown, J.S., and Anderson, A.R.A. (2019). The impact of proliferation-migration tradeoffs on phenotypic evolution in cancer. Sci. Rep. 9, 2425. https://doi.org/10.1038/s41598-019-39636-x.

3. Vittadello, S.T., McCue, S.W., Gunasingh, G., Haass, N.K., and Simpson, M.J. (2020). Examining Go-or-Grow Using Fluorescent Cell-Cycle Indicators and Cell-Cycle-Inhibiting Drugs. Biophys. J. 118, 1243–1247. https://doi.org/10.1016/j.bpj.2020.01.036.

4. Garay, T., Juhász, É., Molnár, E., Eisenbauer, M., Czirók, A., Dekan, B., László, V., Hoda, M.A., Döme, B., Tímár, J., et al. (2013). Cell migration or cytokinesis and proliferation?–revisiting the "go or grow" hypothesis in cancer cells in vitro. Exp. Cell. Res. 319, 3094–3103. https://doi.org/10.1016/j.yexcr.2013.08.018.

5. Hatzikirou, H., Basanta, D., Simon, M., Schaller, K., and Deutsch, A. (2012). Go or grow': the key to the emergence of invasion in tumour progression? Math. Med. Biol. 29, 49–65. https://doi.org/10.1093/imammb/dqq011.

6. Gude, S., Pinçe, E., Taute, K.M., Seinen, A.-B., Shimizu, T.S., and Tans, S.J. (2020). Bacterial coexistence driven by motility and spatial competition. Nature 578, 588–592. https://doi.org/10.1038/s41586-020-2033-2.

7. Kuhn, T., Mamin, M., Bindschedler, S., Bshary, R., Estoppey, A., Gonzalez, D., Palmieri, F., Junier, P., and Richter, X.-Y.L. (2022). Spatial scales of competition and a growth–motility trade-off interact to determine bacterial coexistence. R. Soc. Open Sci. 9, 211592.

8. Shoval, O., Sheftel, H., Shinar, G., Hart, Y., Ramote, O., Mayo, A., Dekel, E., Kavanagh, K., and Alon, U. (2012). Evolutionary trade-offs, Pareto optimality, and the geometry of phenotype space. Science 336, 1157–1160.

9. Shen-Orr, S.S., Milo, R., Mangan, S., and Alon, U. (2002). Network motifs in the transcriptional regulation network of Escherichia coli. Nat. Genet. 31, 64–68. https://doi.org/10.1038/ng881.

10. Santos-Zavaleta, A., Salgado, H., Gama-Castro, S., Sánchez-Pérez, M., Gómez-Romero, L., Ledezma-Tejeida, D., García-Sotelo, J.S., Alquicira-Hernández, K., Muñiz-Rascado, L.J., Peña-Loredo, P., et al. (2019). RegulonDB v 10.5: tackling challenges to unify classic and high throughput knowledge of gene regulation in E. coli K-12. Nucleic. Acids. Res. 47, D212–D220.

11. Botsford, J.L., and Harman, J.G. (1992). Cyclic AMP in prokaryotes. Microbiol. Rev. 56, 100–122.

12. Liu, C., Sun, D., Zhu, J., Liu, J., and Liu, W. (2020). The regulation of bacterial biofilm formation by cAMP-CRP: a mini-review. Front. Microbiol. 11, 802.

13. Dillon, S.C., and Dorman, C.J. (2010). Bacterial nucleoid-associated proteins, nucleoid structure and gene expression. Nat. Rev. Microbiol. 8, 185–195. https://doi.org/10.1038/nrmicro2261.

14. Bradley, M.D., Beach, M.B., de Koning, A.P.J., Pratt, T.S., and Osuna, R. (2007). Effects of Fis on Escherichia coli gene expression during different growth stages. Microbiology 153, 2922–2940.

15. Laurent-Winter, C., Ngo, S., Danchin, A., and Bertin, P. (1997). Role of Escherichia Coli Histone-Like Nucleoid-Structuring Protein in Bacterial Metabolism and Stress Response. Eur. J. Biochem. 244, 767–773. https://doi.org/10.1111/j.1432-1033.1997.00767.x.

16. Moor, H., Teppo, A., Lahesaare, A., Kivisaar, M., and Teras, R. (2014). Fis overexpression enhances Pseudomonas putida biofilm formation by regulating the ratio of LapA and LapF. Microbiology 160, 2681–2693.

17. Browning, D.F., and Busby, S.J.W. (2016). Local and global regulation of transcription initiation in bacteria. Nat. Rev. Microbiol. 14, 638–650.

18. Fitzgerald, D.M., Bonocora, R.P., and Wade, J.T. (2014). Comprehensive mapping of the Escherichia coli flagellar regulatory network. PLoS Genet. 10, e1004649. https://doi.org/10.1371/journal.pgen.1004649.

19. Pesavento, C., Becker, G., Sommerfeldt, N., Possling, A., Tschowri, N., Mehlis, A., and Hengge, R. (2008). Inverse regulatory coordination of motility and curli-mediated adhesion in Escherichia coli. Genes. Dev. 22, 2434–2446. https://doi.org/10.1101/gad.475808.

20. Mika, F., and Hengge, R. (2014). Small RNAs in the control of RpoS, CsgD, and biofilm architecture of Escherichia coli. RNA Biol. *11*, 494–507. https://doi.org/10.4161/rna.28867.

21. Bikard, D., Jiang, W., Samai, P., Hochschild, A., Zhang, F., and Marraffini, L.A. (2013). Programmable repression and activation of bacterial gene expression using an engineered CRISPR-Cas system. Nucleic Acids Res. *41*, 7429–7437.

22. Adler, J. (1966). Chemotaxis in Bacteria. Science *153*, 708–716. https://doi.org/10.1126/science.153.3737.708.

23. Lauffenburger, D., Kennedy, C., and Aris, R. (1984). Traveling bands of chemotactic bacteria in the context of population growth. Bull. Math. Biol. *46*, 19–40. https://doi.org/10.1016/S0092-8240(84)80033-6.

24. Wiser, M.J., and Lenski, R.E. (2015). A comparison of methods to measure fitness in Escherichia coli. PLoS One *10*, e0126210.

25. Fraebel, D.T., Mickalide, H., Schnitkey, D., Merritt, J., Kuhlman, T.E., and Kuehn, S. (2017). Environment determines evolutionary trajectory in a constrained phenotypic space. Elife *6*, e24669.

26. Yi, X., and Dean, A.M. (2016). Phenotypic plasticity as an adaptation to a functional trade-off. Elife *5*, e19307.

27. Macía, J., Solé, R.V., and Elena, S.F. (2012). THE CAUSES OF EPISTASIS IN GENETIC NETWORKS. Evolution *66*, 586–596. https://doi.org/10.1111/j.1558-5646.2011.01451.x.

28. Nghe, P., Kogenaru, M., and Tans, S.J. (2018). Sign epistasis caused by hierarchy within signalling cascades. Nat. Commun. *9*, 1451. https://doi.org/10.1038/s41467-018-03644-8.

29. Omholt, S.W., Plahte, E., Øyehaug, L., and Xiang, K. (2000). Gene regulatory networks generating the phenomena of additivity, dominance and epistasis. Gene *155*, 969–980.

30. de Vos, M.G.J., Poelwijk, F.J., Battich, N., Ndika, J.D.T., and Tans, S.J. (2013). Environmental Dependence of Genetic Constraint. PLoS Genet. *9*, e1003580. https://doi.org/10.1371/journal.pgen.1003580.

31. Martínez-Antonio, A., and Collado-Vides, J. (2003). Identifying global regulators in transcriptional regulatory networks in bacteria. Current *6*, 482–489.

32. Liu, R., Liang, L., Freed, E.F., Choudhury, A., Eckert, C.A., and Gill, R.T. (2020). Engineering regulatory networks for complex phenotypes in E. coli. Nat. Commun. *11*, 4050. https://doi.org/10.1038/s41467-020-17721-4.

33. Baier, F., Gauye, F., Perez-Carrasco, R., Payne, J.L., and Schaerli, Y. (2023). Environment-dependent epistasis increases phenotypic diversity in gene regulatory networks. Sci. Adv. *9*, eadf1773. https://doi.org/10.1126/sciadv.adf1773.

34. Boguñá, M., Bonamassa, I., De Domenico, M., Havlin, S., Krioukov, D., and Serrano, M.Á. (2021). Network geometry. Nat. Rev. Phys. *3*, 114–135. https://doi.org/10.1038/s42254-020-00264-4.

35. Torres-Sosa, C., Huang, S., and Aldana, M. (2012). Criticality Is an Emergent Property of Genetic Networks that Exhibit Evolvability. PLoS Comput. Biol. *8*, e1002669. https://doi.org/10.1371/journal.pcbi.1002669.

36. Peebo, K., Valgepea, K., Maser, A., Nahku, R., Adamberg, K., and Vilu, R. (2015). Proteome reallocation in Escherichia coli with increasing specific growth rate. Mol. Biosyst. *11*, 1184–1193. https://doi.org/10.1039/C4MB00721B.

37. Galis, F., and Metz, J.A.J. (2007). Evolutionary novelties: the making and breaking of pleiotropic constraints. Integr. Comp. Biol. *47*, 409–419.

38. Hu, D., Li, Y., Zhang, D., Ding, J., Song, Z., Min, J., Zeng, Y., and Nie, C. (2022). Genetic trade-offs between complex diseases and longevity. Aging Cell *21*, e13654.

39. Tang, J., Huang, M., He, S., Zeng, J., and Zhu, H. (2022). Uncovering the extensive trade-off between adaptive evolution and disease susceptibility. Cell Rep. *40*, 111351.

40. Giese, A., Loo, M.A., Tran, N., Haskett, D., Coons, S.W., and Berens, M.E. (1996). Dichotomy of astrocytoma migration and proliferation. Int. J. Cancer. *67*, 275–282.

41. Dhruv, H.D., McDonough Winslow, W.S., Armstrong, B., Tuncali, S., Eschbacher, J., Kislin, K., Loftus, J.C., Tran, N.L., and Berens, M.E. (2013). Reciprocal activation of transcription factors underlies the dichotomy between proliferation and invasion of glioma cells. PLoS One *8*, e72134.

42. Bien, S.A., and Peters, U. (2019). Moving from one to many: insights from the growing list of pleiotropic cancer risk genes. Br. J. Cancer. *120*, 1087–1089.

43. Gough, P., and Myles, I.A. (2020). Tumor necrosis factor receptors: pleiotropic signaling complexes and their differential effects. Front. Immunol. *11*, 585880.

44. Hausser, J., Szekely, P., Bar, N., Zimmer, A., Sheftel, H., Caldas, C., and Alon, U. (2019). Tumor diversity and the trade-off between universal cancer tasks. Nat. Commun. *10*, 5423.

45. Nguyen, B., Fong, C., Luthra, A., Smith, S.A., DiNatale, R.G., Nandakumar, S., Walch, H., Chatila, W.K., Madupuri, R., Kundra, R., et al. (2022). Genomic characterization of metastatic patterns from prospective clinical sequencing of 25,000 patients. Cellule *185*, 563–575.

46. Petit, A.J.R., Guez, J., and Le Rouzic, A. (2023). Correlated stabilizing selection shapes the topology of gene regulatory networks. Genetics *224*, iyad065.

47. Gros, P.-A., Le Nagard, H., and Tenaillon, O. (2009). The evolution of epistasis and its links with genetic robustness, complexity and drift in a phenotypic model of adaptation. Genetics *182*, 277–293.

STAR★METHODS

KEY RESOURCES TABLE

REAGENT or RESOURCE	SOURCE	IDENTIFIER
Bacterial and virus strains		
NEB® Stable Competent *E. coli* (High Efficiency)	New England Biolabs	Cat# C3040I
Escherichia coli (Migula) Castellani and Chalmers	ATCC	Cat# 700926
Chemicals, peptides, and recombinant proteins		
Chloramphenicol	Sigma-Aldrich	Cat# C0378
Kanamycin	Sigma-Aldrich	Cat# K1377
Anhydrotetracycline hydrochloride	Sigma-Aldrich	Cat# 94664
Oligonucleotides		
See Table S3	Integrated DNA Technologies	N.A.
Recombinant DNA		
pdCas9	Addgene	Plasmid #46569
Software and algorithms		
Python	Python Software Foundation	Version 3.10.9
The code to perform the simulations and reproduce the figures	Zenodo	https://doi.org/10.5281/zenodo.10201172
Data		
Data used in figures	Zenodo	https://doi.org/10.5281/zenodo.10201172
Raw data	lead contact	N.A.

EXPERIMENTAL MODEL AND STUDY PARTICIPANT DETAILS

Microbe strains used

Escherichia coli K-12 MG1655 was used for all fitness experiments. *Escherichia coli* NEB Stable Competent E. coli (High Efficiency) (Catalog #C3040I) was used for creation of all vectors.

Growth conditions of cultures

The host strain for all pCRRNA vectors is MG1655 with the pdCas9 vector from Stanley Qi (provided by Lun Cui and David Bikard). Glycerol stocks of each culture were streaked onto individual Lysogeny Broth (LB) agar plates containing 34 μg/mL of Chloramphenicol and 50 μg/mL of Kanamycin. Single colonies were inoculated into 2 mL of selected media (either LB or M63 supplemented with 0.4% Glucose or Lactose) containing 34 μg/mL Chloramphenicol and 50 μg/mL Kanamycin. Cultures were placed in a 37°C incubator for 16 h for LB cultures or 24 h for M63 cultures.

METHOD DETAILS

Creation of vectors

pCRRNA mCherry and pCRRNA EGFP were made by Gibson Assembly. PCR was performed on pMD019 (pGFP) and pMD024 (pmCherry) with primers oMD546 and oMD547, and on pCRRNA with primers oMD545 and oMD548. PCR products were purified with a PCR clean-up kit from Macherey-Nagel. Equal molar concentrations of the PCR product were mixed (one from either pMD019 or pMD024 and one from pCRRNA) and 5 μL of the mix was added to 15 μL of Gibson Master mix to create pCRRNA Green and pCRRNA Red respectively. Golden Gate Assembly was used to replace the TrrnB terminator from pMD019 and pMD024 with B0014 as the TrrnB terminator contained 2 BsaI sites. PCR was done on pCRRNA Green and pCRRNA Red with primers oMD609 and oMD610, and on pCKDL with primers oMD607 and oMD608. PCR products were joined with Golden Gate Assembly using BsmBI enzyme to create pCRRNA EGFP and pCRRNA mCherry. pCRRNA mCerulean was created by Gibson Assembly. PCR

was performed on pMD027 (pCerulean) with primers oMD704 and oMD705, and on pCRRNA mCherry with primers oMD706 and oMD707). PCR products were purified with a PCR clean-up kit from Macherey-Nagel. Equal molar concentrations of the PCR product were mixed and 5 μL of mix was added to 15 μL of Gibson Master mix. All vectors were sequenced by GATC Biotech before use.

Growth competition assays

Assays were performed by diluting 220 μL pCRRNA mCherry NT pre-culture into 22 mL of selected media containing 34 μg/mL Chloramphenicol, 50 μg/mL Kanamycin, and 25 ng/mL anhydrotetracycline. A Greiner, 96 Well, PS, F-Bottom, μCLEAR, Black microplate was filled with 198 μL of diluted culture per well. For each pCRRNA EGFP knock down vector, 2 μL of pre-culture was inoculated into 3 individual wells. For the Non-targeting Control strain 'RS, 2 μL of pre-culture was inoculated into 15 individual wells. A volume of 60 μL of mineral oil was added to each well of the microplate. The absorbance at 595 nm, as well as fluorescence at 480/510 nm and 580/610 nm (excitation/emission), were recorded every 10 min for 20 h with a SpectraMax i3x. Microplates were incubated at 37°C and shook for 90 s before and after each measurement. The absolute growth rate of the reference strain was determined by the change in the log2(OD595nm)/time of the exponential growth phase (50mins–170mins in LB, 50mins–230mins in M63). To determine the fitness measurement of each knock down, the ratio of the green and red fluorescence of the strain was divided by the median ratio of the green and red fluorescence of the 12 additional wells for the non-targeting control. Fitness measurements for each knock down were made for LB media, and M63 media containing 0.4% of either glucose or lactose.

Swimming assays

For each knock down, 10 μL of pre-culture was spotted in the middle of 15 mL of selected media soft agar (0.3%) plates. Plates were then incubated at 37°C for either 16 h for LB plates or 24 h for M63 plates. Plates were then imaged using a USB Camera and Python viewer. An image of a non-inoculated plate was subtracted from each image. The fitness was determined by the ratio of the swimming area diameter of each knock down strain to that of the non-targeting control strain.

EVOLUTIONARY SIMULATION

We defined our fitness function as: $F = \lambda g + (1 - \lambda)Sig(k \times (s - s_0))$, where g and s are the growth and swim phenotypic values, respectively. The parameter λ controls the relative importance of both phenotypes in determining fitness, but note that λ itself does not impose a trade-off, it only determines which phenotype has most importance when there is a pre-existing trade-off. $Sig(x) = \frac{1}{1+e^{-x}}$, s_0 is the inflection point of the sigmoid function, and k determines its steepness. For each KD landscape, we have four values of measured growth and four values of measured swim for each pair of genes, allowing us to simulate their dynamics.

We simulated the gene dynamics using the following genetic algorithm with mutation and bottleneck, looped through steps 2–4 for N generations.

(1) Initialization: We initialized a population of P individuals, each randomly assigned to one of the four possible genotypes: RS, local KD, global KD, and double KD.
(2) Mutation: 2% of the population was mutated (strong selection regime). For this subset, we randomly chose one of the two genes and knocked its state either up or down.
(3) Evaluation: We computed the fitness for each individual in the population.
(4) Selection: We implemented a selection process by subsampling the population based on the probability of each individual i:

$$p(i) = \frac{exp\left(\frac{F_i}{T}\right)}{\sum_{j=0}^{n} exp\left(\frac{F_j}{T}\right)},$$ where T represents a fictitious temperature that allows us to adjust the strength of the selection, and j runs over all n genotypes in the population.

For each KD pair, the environment was randomly changed every 200 generations, for a total of 2000 generations at T = 7.

Code

The code is written in Python version 3.10.9 and has been run on a Linux machine with 20 cores 12th Gen Intel(R) Core(TM) i7. A simulation for a population size of 2000 and 2000 generations takes less than a minute. The code to perform the simulations and reproduce the figures is provided at https://doi.org/10.5281/zenodo.10201172, which is in the format of notebooks for the analysis, and Python scripts for the routines.

The routine evo_loop_env_change from the src/evo_four_states.py script performs the evolutionary simulation. It requires the measured phenotypic parameters located in the data directory. The user can choose the population size, the maximum number of generations, the frequency at which the environment is changed, and the mutation rate in the population.

In the output of the simulation routine, the populations as well as the mutations accepted are recorded for each generation in two variables. In these variables, genotypes are encoded in the following way RS = (−1, −1); Delta Local = (1, −1); Delta Global (−1, 1); and double knock down = (1, 1).

QUANTIFICATION AND STATISTICAL ANALYSIS

Computation of relative growth rates

Fitness differences between a mutant and the reference strain (respectively denoted with superscripts 'm' and 'w') are measured as the slope of the function:

$$\log\left(\frac{F_r^m}{F_b^w}\right) - \log\left(\frac{F_r^w}{F_b^w}\right)$$

where F is the fluorescence measured over time with indices 'r' and 'b' for mCherry and CFP fluorescent reporter strains. To show that this measurement is appropriate, let us first evaluate how a fluorescent intensity F_i depends on time. First, given the fluorescence intensity a_i per protein of type 'i' and a maturation time τ_i, fluorescence is delayed compared to the number of accumulated fluorescent proteins N_i, so that:

$$F_i(t) = a_i N_i(t - \tau_i) \qquad \text{(Equation 1)}$$

Second, during steady exponential growth at rate λ_i, proteins are produced at a rate proportional to the total mass of the cell, and considering the degradation rate d_i:

$$\frac{dN_i}{dt} = N_i^0 e^{\lambda_i t} - d_i N_i$$

The solution to the above equation is:

$$N_i(t) = N_i^0 e^{\lambda_i t} \frac{1 - e^{-(\lambda_i + d_i)t}}{\lambda_i + d_i}$$

The term $e^{-(\lambda_i + d_i)t}$ fades exponentially compared to 1, with a characteristic time shorter than a cell cycle by definition of λ_i. Consequently, after a few cycles, N_i is very well approximated as

$$N_i(t) \approx \frac{N_i^0 e^{\lambda_i t}}{\lambda_i + d_i}$$

In combination with 1, this gives:

$$F_i(t) = \frac{a_i N_i^0}{\lambda_i + d_i} e^{\lambda_i (t - \tau_i)}$$

The ratio between the intensity of any two fluorescent signals is:

$$\log\left(\frac{F_2}{F_1}\right) = \left[\frac{a_2 N_2^0}{a_1 N_1^0} \frac{\lambda_1 + d_1}{\lambda_2 + d_2} + \lambda_1 \tau_1 - \lambda_2 \tau_2\right] + (\lambda_2 - \lambda_1)t$$

Therefore, the slope $(\lambda_2 - \lambda_1)$ as a function of time corresponds to the fitness difference, any dependence in maturation time, initial amount, and degradation rate being accounted for by the bracketed constant term. Still, a fluorescent strain may be affected by a growth cost c_i specifically associated with the fluorescent protein being expressed, so that it measured fitness λ_i differs from its fitness μ_i in the absence of the reporter:

$$\lambda_i = \mu_i - c_i$$

The contribution of c_i is removed when computing the slope of $\log\left(\frac{F_r^m}{F_b^w}\right) - \log\left(\frac{F_r^w}{F_b^w}\right)$, as, given the above, this slope equals the fitness difference independently of the construct and initial conditions:

$$\left(\lambda_r^m - \lambda_b^w\right) - \left(\lambda_b^w - \lambda_r^w\right) = \left(\mu^m - c_r^m - \mu^w + c_b^w\right) - \left(\mu^w - c_b^w - \mu^w + c_r^w\right) = \mu^m - \mu^w$$

Statistical methods used

For each condition, 3 independent biological replicates were grown from single colonies. For each biological replicate, 3 independent technical replicates were performed for each experiment, for a total number of replicates for each condition of $n = 9$. Fitness data is presented as the median of all biological and technical replicates ($n = 9$) for a given condition. Error is represented as Standard Error of the Median (SEM). Significance is determined by Welch's t-test with a p value of ≤ 0.05.